SURFACE AND INTERFACE ANALYSIS
Surf. Interface Anal. 2002; **33**: 126–136

SIA

Mesophase-derived nucleic acid (peptide) self-organizations visualized by scanning force microscopy

Walter-Veselý Meister,[1] Christian Bohley,[1] Sabine Lindau,[1] Ulrich Gromann,[1] Stefan Naumann,[2] Bernd Herrmann,[1] Sergej I. Kargov,[4] Torsten Martini,[3] Jochen Barthel[3] and Siegfried Hoffmann[1]*

[1] Institute of Biochemistry, Martin Luther University Halle-Wittenberg, D-06120 Halle (Saale), Germany
[2] Institute of Chemistry, Martin Luther University Halle-Wittenberg, D-06120 Halle (Saale), Germany
[3] Max Planck Institute of Microstructure Physics, D-06120 Halle (Saale), Germany
[4] Moscow State University, Faculty of Chemistry, 119899 Moscow, Russia

Received 6 November 2000; Revised 19 June 2001; Accepted 8 July 2001

For approaching biomesogen self-organizations in nucleic acid (peptide) assemblies from the perspective of interacting individual macromolecules and their integrating collective mesophase organizations, DNA duplex as well as RNA duplex, triplex, quadruplex and duplex/peptide domains and microdomains have been visualized as graphite surface adlayers by scanning force microscopy. Derived from corresponding mesophase designs, the adlayer imagings of dsDNA, dsRNA and qsRNA reveal aligned supramolecular bundles that follow self-organizational strategies within the adlayer/interface restrictions. For tsRNA and dsRNA/oligo- and polypeptide variations more complex adlayer organizations are observed. Copyright © 2002 John Wiley & Sons, Ltd.

KEYWORDS: nucleic acids; biomesogenic preordering; self-organization; polarizing microscopy; scanning force microscopy (SFM)

INTRODUCTION

It seems that life originated with optimizable amphiphilic patterns in complex tensions of liquid/solid interfaces.[1,2] It was the mesogenic constituents of the grand amphiphilic patterns of life that provided decisive prerequisites for the projection of individual molecular facilities into the structural and functional amplifications of cooperative and dynamic (bio)mesogen domain ensembles within the growing complexity of self-sustaining patterns.[1–4]

Although life from its beginning appears intrinsically inflicted by inherent structure/phase dualities,[2] scientific investigations met with difficulties in approaching central regions where molecular structural amplifications and phase/microphase/cluster reductions establish elementary dynamic units of developmental supramolecular biomesogen organizations[1–12,14,15] (Figs 1 and 2). Solid- and liquid (solution)-phase studies outclassed promising mesophase areas in-between.[6,7,13] The first hesitating biopolymer mesophase elucidations tried to avoid threatening complexities by embarking preferentially on plain and clearcut experimental conditions.[25–33] Life, however, from its very beginning, has been ruled by indeterministics rather than deterministics and thus many derivations from beautiful deterministic scientific experiments will end their causality chains where life in reality would start.[1–4,20–24,33]

Trials to overcome methodological shortcomings and disciplinary limitations have to face life in all its complexities, linking prebiotic outsets with the last species optimization strategies.[1]

Among the recent achievements to deal with supramolecular biomesogen complexities, molecular-resolving and dynamically extended microscopies offer intriguing insights into the sequences from preintelligent self-organizations over organismic perfectionism—even up to the magic problems of human consciousness. Still somewhat in their infancies, scanning probe microscopies (SPM/SXM), especially scanning force (SFM) and scanning tunnelling microscopy (STM), approach the dualism between supramolecular constituents and biomesogen operation modes in the complex hierarchies of life.[1–4]

*Correspondence to: S. Hoffmann, Institute of Biochemistry, Martin Luther University Halle-Wittenberg, Kurt-Mothes-Str. 3, D-06120 Halle (Saale), Germany.
E-mail: hoffmann@biochemtech.uni-halle.de
Contract/grant sponsor: Saxony-Anhalt Ministry of Culture and Education.
Contract/grant sponsor: Ministry for Science and Research (Saxony-Anhalt).
Contract/grant sponsor: Funds of Chemical Industries.
Contract/grant sponsor: National Employment Office Halle/Saale.
Contract/grant sponsor: EU-INTAS Projects.
Contract/grant sponsor: DAAD-Eastpartnerships.

DOI: 10.1002/sia.1176

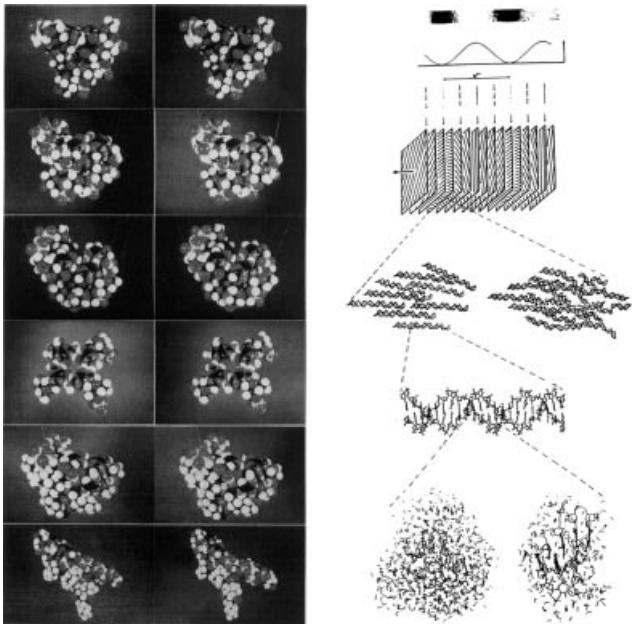

Figure 1. Basic nucleic acid geometries (left part, top-down) in Corey–Pauling-Kultun (CPK) presentation[1,2,6,7,13,17] — dsDNA, dsRNA, tsRNA, qsRNA[$(G)_n$] and hypothetical dsRNA/$(L\text{-Lys})_n$ complexations with β-stranded $(Lys)_n$ — fitting salt- and hydrogen-bonding networks within the shallow grooves of A-RNA and Olson-RNA,[4,16] compared (right part, top-down) with mesophase reduction via microphase (top-down) and structural amplifications via macromolecules (bottom-up), centering in the (pre)biologically relevant areas of supramolecular (bio)mesogen organizations.[1–4,15,17–24]

MATERIALS AND METHODS

Poly(deoxy)nucleotides and peptides

Poly(deoxy)nucleotides and oligo- and polypeptides (DNA: Reanal; RNAs: Serva, potassium salts; polypeptides: Serva, HBr salts) include high-molecular-weight polydispersed chicken-erythrocyte DNA (ch-DNA) ($\varepsilon_{260} = 6.6 \times 10^3$), polyuridylic acid $(U)_n$ ($S_{20,w} = 5.7$, $\varepsilon_{260} = 9.35 \times 10^3$), polyadenylic acid $(A)_n$ ($S_{20,w} = 8.8$, $\varepsilon_{258} = 9.8 \times 10^3$), polyguanylic acid $(G)_n$ ($S_{20,w} = 7.8$, $\varepsilon_{260} = 9.9 \times 10^3$), L-(tetralysyl)lysine and poly-L-lysine 2000 ($M_r = 2–5$ kDa), 6000 ($M_r = 6–9$ kDa), 10 000 ($M_r = 10–20$ kDa) and 15 000 ($M_r = 15–30$ kDa).

The T_m measurements for poly(deoxy)nucleotides were carried out in sterile bidistilled water by increasing the temperature at a rate of 1.0 °C min^{-1}. with the help of a Lambda2 spectrometer equipped with a PTP-1 Peltier temperature control device.

The ch-DNA was swollen in sterile bidistilled water (4 °C, 3 days) and the diluted aqueous solution (0.1 mM in 1 mM NaCl) then analysed by T_m melting curves ($T_m = 69$ °C).

The aqueous double-stranded (ds) RNA solutions of $(A)_n \cdot (U)_n$ were prepared by mixing equimolar amounts of the preswollen (bidistilled water, 4 °C, 3 days), diluted and denaturated (80 °C, 5 min) polydispersed RNA single strands in nuclease-free vessels. After hybridization (4 °C, 5 days) the samples were dissolved in the buffer solution and analysed by their T_m melting behaviour (0.1 mM RNA-p in PBS buffer of 0.01 M phosphate and 0.15 M NaCl, pH 7.0; $\varepsilon_{260} = 6.1 \times 10^3$; $T_m = 56$ °C).

For the triple-stranded (ts) RNA solution of $(A)_n \cdot 2(U)_n$ an additional equimolar amount of the denaturated (80 °C, 5 min) $(U)_n$ single-strand solution was added to the above-prepared $(A)_n \cdot (U)_n$ solution at 15 °C. The solution was incubated (4 °C, 7 days) before analysis (0.1 mM RNA-p in PBS buffer of 0.01 M phosphate and 0.15 M NaCl, pH 7.0; $T_m = 58$ °C).

The quadruplex of polyguanylic acid $(G)_n$ was prepared by heating the preswollen (bidistilled water, 4 °C, 3 days) aqueous $(G)_n$ solution (1 mM, 90 °C, 5 min) and slowly cooling down. The polyguanylic acid–tetraplex $(G)_n \cdot (G)_n \cdot (G)_n \cdot (G)_n$ solution shows no T_m below 95 °C (0.1 mM RNA-p in PBS buffer of 0.01 M phosphate and 0.15 M NaCl, pH 7.0).

The DNA– and RNA–peptide complexes of chicken DNA as well as polyuridylic · polyadenylic acid duplex and triplex combinations (potassium salts) with oligo- and poly-L-lysines (HBr salts: L-(tetralysyl)lysine and poly-L-Lys-2000/6000/10000/15000) were prepared at 20 °C by mixing the buffered aqueous nucleic acid solutions (0.1 mM RNA-p in PBS buffer of 0.01 M phosphate and 0.15 M NaCl, pH 7.0) with the indicated equivalent of oligo- and poly-L-lysines diluted in a small amount of water. The complexes were analysed by their T_m melting behaviour: ch-DNA/0.1$(L\text{-Lys})_5$, 72 °C;

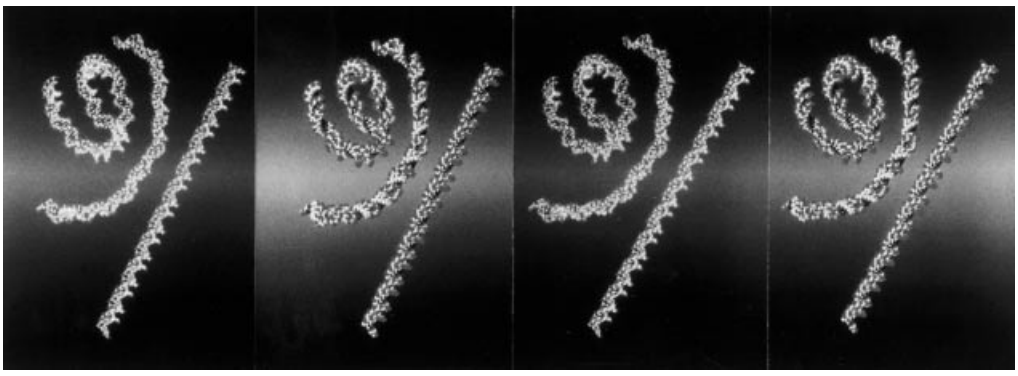

Figure 2. Nucleic acid geometries as molecular building blocks of biomesogen organizations (left to right) in skeleton and CPK illustrations:[1,2,6,7,16,34–42] dynamics of dsDNA with asymmetric counter-ion cloud distribution (centre), approaching suprahelical circular (top left) from linear (bottom right) dsDNA.

$(U)_n \cdot (A)_n$/0.1(L-Lys)$_5$, 65 °C; $(2U)_n \cdot (A)_n$/0.1(L-Lys)$_5$, 65 °C; $(U)_n \cdot (A)_n$/0.05/0.1/0.2(L-Lys2000), 62/62/67 °C; $(U)_n \cdot (A)_n$/0.1(L-Lys6000), 64 °C; $(U)_n \cdot (A)_n$/0.1(L-Lys10000), 64 °C; $(U)_n \cdot (A)_n$/0.1(L-Lys15000), 63 °C.

Polarizing light microscopy

For polarizing light microscopy studies (Figs 3 and 4), the lyophilized samples were swollen in sterile bidistilled water (4 °C, 3 days). Then the solutions were filled up with buffer solutions (ch-DNA samples: 1 mM NaCl, RNA and RNA(peptide) samples: 0.01 M phosphate, 0.15 M NaCl) to reach DNA and RNA(peptide) start concentrations of ~100 mg ml^{-1}. After that, a 10–15 µl droplet of each sample solution was deposited between a partially sealed slide and coverslip and observed by employing a Leitz Labor Lux 12S polarizing microscope equipped with a Hitachi KP-551 video colour camera (crossed polars, magnification rate 536×). The progressive increase of the sample concentration was obtained by controlled evaporation of the solvent, yielding a continuous concentration gradient. The textures were observed after a few minutes to a few hours at room temperature.

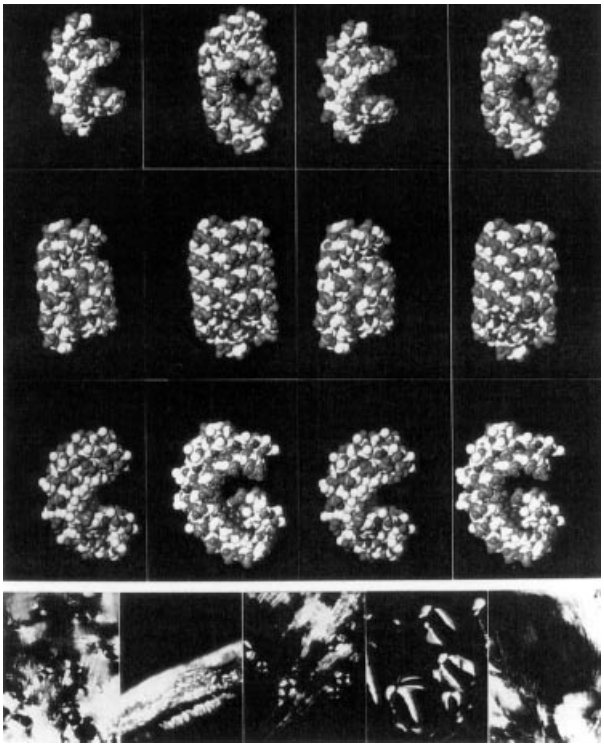

Figure 3. Biomesogen nucleic acid (peptide) organizations (top) and their mesophase textures (bottom). Nucleic acid (peptide) geometries (left to right and top to bottom): B-DNA and A-RNA duplex, RNA triplex and $(G)_n$-quadruplex[1–4,6,7,16,17,33–35]; DNA- and RNA/(peptide β-sheet) evolutionary models for nucleic acid–peptide interactions.[40–42,63] Sequence-corresponding liquid crystal textures in individual evolutions between cholesteric and columnar design (left to right and top to bottom): ch-DNA, mosaics of fingerprints; $(U)_n \cdot (A)_n$, cholesteric/columnar terraces; $(U)_n \cdot (A)_n \cdot (U)_n$ and $(G)_n \cdot (G)_n \cdot (G)_n \cdot (G)_n$, cholesteric spherulites: $(U)_n \cdot (A)_n$/0.1(L-Lys)$_5$, mosaics of fingerprints (magnification 536×).

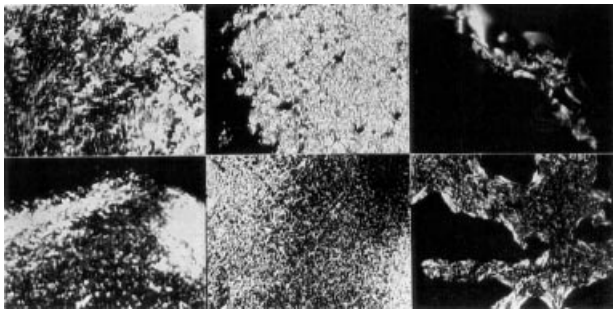

Figure 4. Comparison of nucleic acid–peptide mesophase variations (left to right and top to bottom): $(U)_n \cdot (A)_n$, multiple cholesteric mosaics; L-Lys-2000, unspecific cholesteric appearances; $(U)_n \cdot (A)_n \cdot (U)_n$, cholesteric/columnar transitions; $(U)_n \cdot (A)_n$/0.1(L-Lys)$_5$, cholesteric/columnar patterns; $(U)_n \cdot (A)_n$/0.1 L-Lys-2000, unspecific complex textures; $(U)_n \cdot (A)_n$/0.1 L-Lys-10 000, cholesteric/columnar patterns (magnification 536×).

Scanning force microscopy (SFM)

The SFM images (Figs 5–7) were collected at room temperature in air using the commercially available Nanoscope III instrument (cantilevers 200 µm long, pyramidal tips of silicon nitride, tip radii 4–40 nm, spring constant 0.06 N m^{-1}). Highly oriented pyrolytic graphite (HOPG) was used as the substrate. For sample preparation, 20 µl of a diluted solution of each nucleic acid (peptide) complex in water were poured slowly across the substrate surface of freshly cleaved HOPG at room temperature, allowing for evaporation as indicated for UV mesophase investigations. The nucleic acid/peptide images were obtained in constant force mode at 15–20 nN net repulsive force, collecting the scans from left to right with a 512 × 512 pixel information density at scan rates of 3.1 Hz for DNA and 1.7 Hz for RNA(peptide) complexes. All images are presented as raw data except for flattening.

Molecular modelling

Both B-DNA and A-RNA (peptide) models (Figs 2, 3 and 8) have been generated according to Brookhaven Protein Data Bank on Silicon Graphics workstations using HAMOG and SYBYL 6.2. programs. Evolution of DNA (Fig. 2) under the conditions of different sidewise helical counter-ion distribution[42] (left side, 0.5 eV, right side, 1.0 eV) has been computed with the force-field MD program Amber 5.0, starting with pure DNA at 67 K up to 70 K (680 ps–0.5 fs, stepwise). Simulations are without constraints, *nVT* ensemble, cut-off radii 10 Å and non-bonded list actualized at every simulation step.

RESULTS AND DISCUSSIONS

Solid-phase physics unravelled the statics and, to a certain degree, foreseeable dynamics of life's informational component.[1–9] Liquid-phase (solution) experiments elucidated its single-molecule operation modes.[1–15,34,42] Late, self-organizational facilities redirected the extreme views to the spectra of diverse mesophase areas.[1–4,10–12] Volume-phase

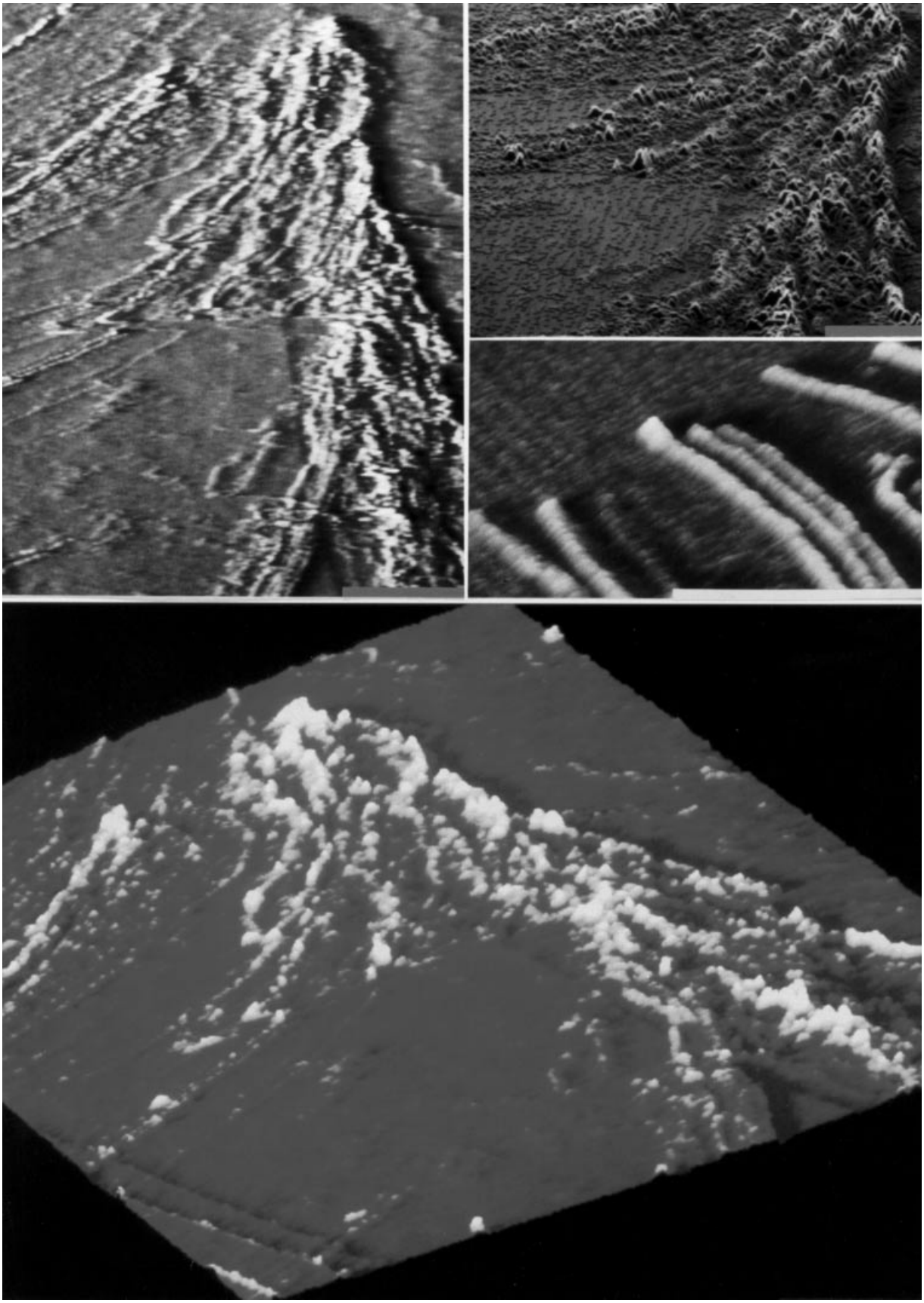

Figure 5. Scanning force microscopy visualizations of polydispersed chicken erythrocyte DNA/HOPG adlayer domains and microdomains (left to right and top to bottom): two- and three-dimensional overall views; three-dimensional single-molecule imaging; three-dimensional overall presentation. Scale: 0.25 μm light bar; 1 μm dark bars.

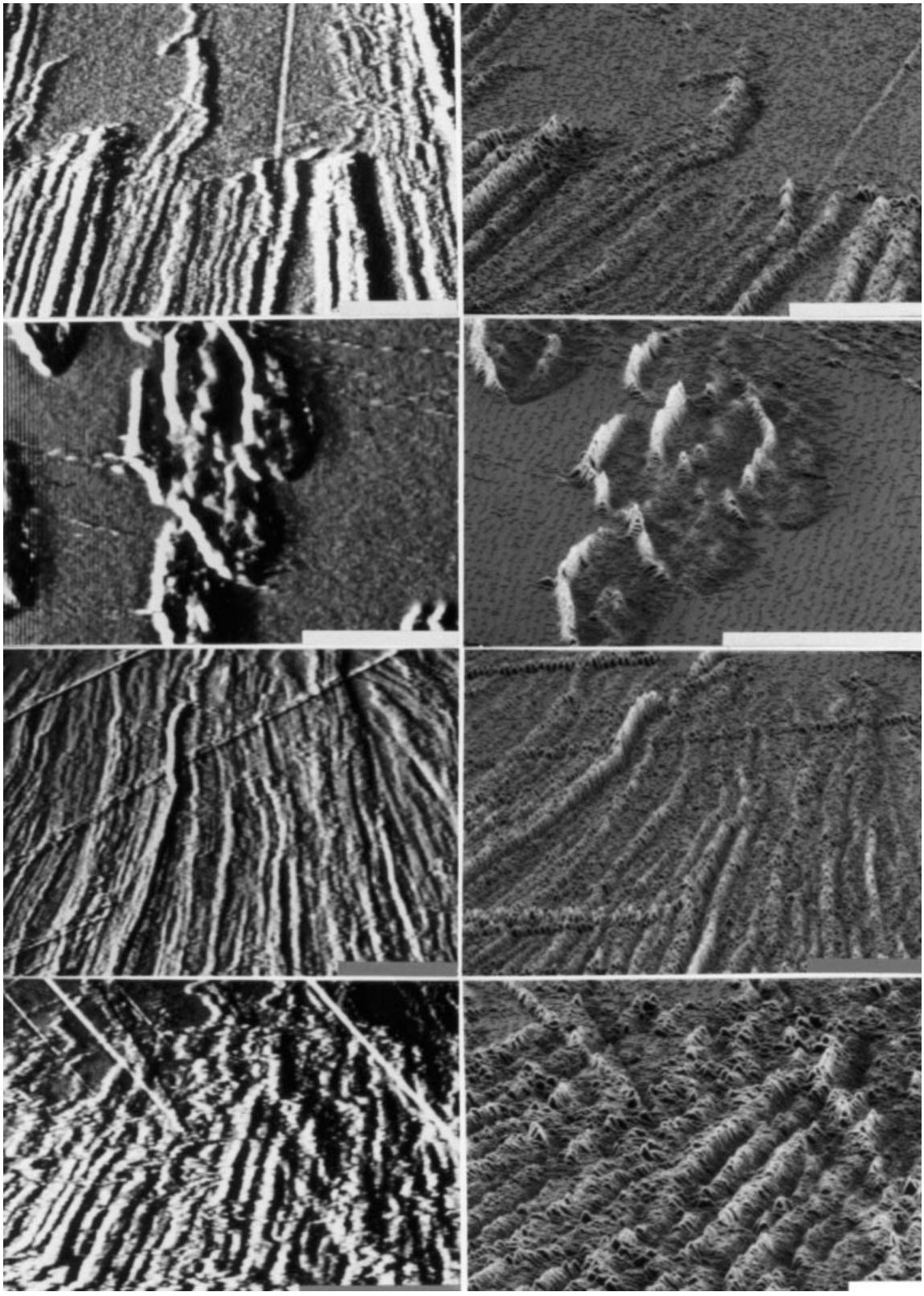

Figure 6. Scanning force microscopy visualizations of ds/ts/qsRNA and dsRNA/short peptide organizations in two-dimensional (left) and three-dimensional (right) presentations (left to right and top to bottom): $(U)_n \cdot (A)_n$ duplex; $(U)_n \cdot (A)_n \cdot (U)_n$ triplex; $(G)_n \cdot (G)_n \cdot (G)_n \cdot (G)_n$ quadruplex and $(U)_n \cdot (A)_n/(L\text{-Lys})_5$. Scale: 0.25 μm light bars; 1 μm dark bars.

investigations yielded more indirect insights into the three-dimensional statics and dynamics of large (idealized) molecular ensembles.[1–5,20–33,48–66] Langmuir–Blodgett approaches, within two-dimensional lateral mesophase extensions, vertically reached the basic operational units of biomesogen nucleic acid/protein/membrane logic blocks.[2,10,24,67] In both cases, SFM and STM seemed promising[68–73] to direct our, so far, statically and dynamically limited insights to basal nano-

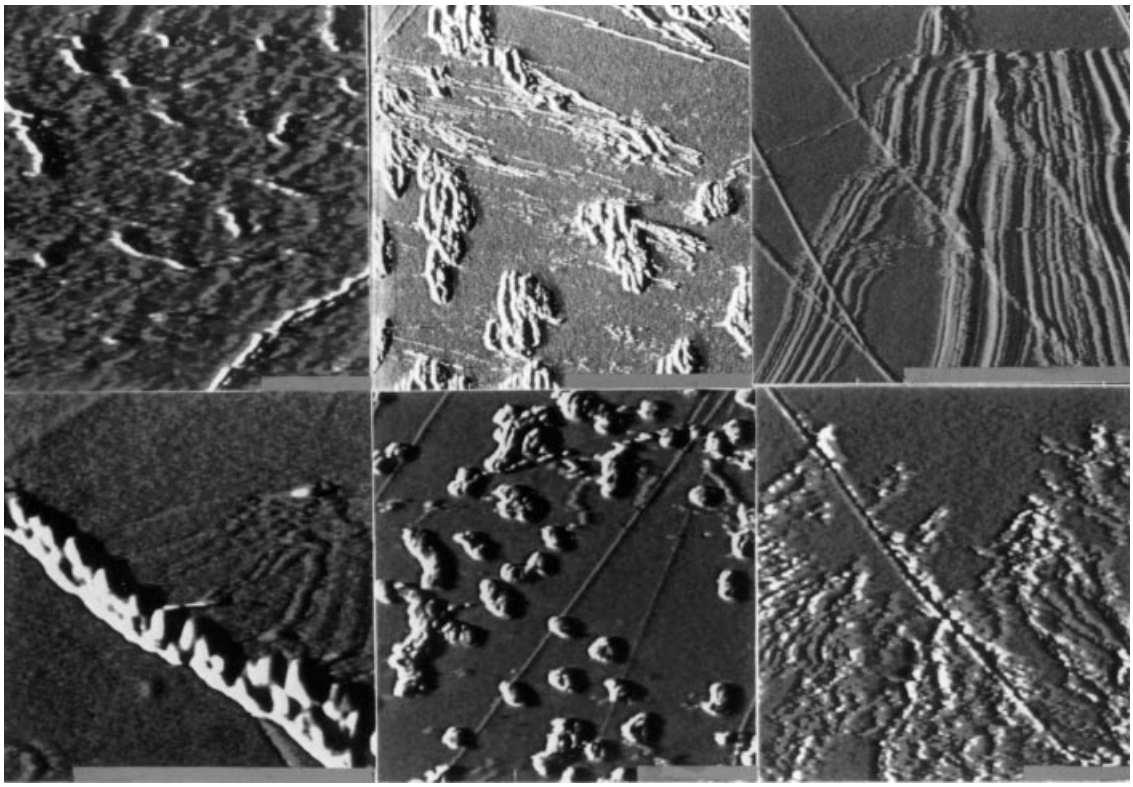

Figure 7. Scanning force microscopy images of dsRNA/peptide variations in two-dimensional presentations (left to right and top to bottom): L-Lys-2000; $(U)_n \cdot (A)_n \cdot (U)_n$; $(U)_n \cdot (A)_n$; $(U)_n \cdot (A)_n$/0.1 L-Lys-2000; $(U)_n \cdot (A)_n$/0.1 L-Lys-6000; $(U)_n \cdot (A)_n$/0.1 L-Lys-10 000. Scale: 1 μm dark bars.

and subnanoscales. In first attempts to visualize supramolecular (bio)mesogen organizations derived from governing mesophase designs, we have carried out corresponding measurements with the help of SFM, STM, polarized light microscopy, differential scanning calorimetry, x-ray diffraction and Langmuir–Blodgett techniques.[74–82]

In the special case here, we tried to enlarge insights into mesophase-derived nucleic acid–peptide adlayer organizations and to link not only ensemble- and individuality-orientated methodologies but to direct the first steps to the continuing approaches for preintelligent organizations on their way up to consciousness[1,2] (Figs 1 and 2).

Contrary to the mainstream of mesophase elucidations of nucleic acids, which so far aimed at distinct phase-diagram relationships promoted by easily surveyable uniform molecular prerequisites as to shape, design and supporting solution conditions, we concentrated on the more difficult to handle processings of polydispersed entities in prebiotically and biologically relevant aqueous solutions. Hereby, each sample represents, to a certain degree, a well-expressed individuality of its own that tries to follow milieu-dependent processings by complex individual mesophase space–time adjustments and adaptations.

Dispensing with these exact differentiations in well-expressed texture appearances and transition sequences that contradict probabilistic evolutionary causes, we tried to cope with those developmental strategies by SFM sights that might forward both molecular and phase/microphase elucidations determining the central parts of supramolecular biomesogen organizations.

Poly(deoxy)nucleotide (peptide) samples and their mesophases — analyzed by polarizing light microscopy

Analyses of the prepared aqueous sample solutions of high-molecular-weight polydispersed ch-DNA as well as $(U)_n \cdot (A)_n$ duplexes, $(U)_n \cdot (A)_n \cdot (U)_n$ triplexes and $(G)_n \cdot (G)_n \cdot (G)_n \cdot (G)_n$ tetraplexes for RNA organizations by T_m melting curves confirm earlier results, including detailed phase diagrams for the $(U)_n/(A)_n$ duplex/triplex variants.[1,6,7,13,16–18,33–41] The ch-DNA/$(L\text{-Lys})_n$ complexations, as well as the differently stranded RNA/$(L\text{-Lys})_n$ combinations meet the general expectations for peptide-based additional stabilizations according to the T_m shifts. Uncertainties about the underlying, molecular models limit more far-reaching suggestions as to structural interdependences.[1,2,6,7,16,27,33–42,63]

Because nucleic acid organizations played crucial (pre)biotic roles in RNA and RNA–DNA–protein world developments[1–9,13–24] and forwarded *in vivo* developments into highly operable condensed organismic forms, as in cells, cell nuclei, genetic materials, ribosomes, mitochondria and other biological objects, up to the consciousness patterns of our central nervous systems,[1,2] the formation of lyo-, thermo- and amphotropic mesophases in concentrated aqueous solutions of these semi-rigid macromolecules and their experimental investigations in the field of complex nucleic acid biomesogen systems have received growing interest.[1–4,20–33,44–67]

The texture observations presented here of nucleic acid (peptide) complexations (Figs 3 and 4) are indicative of the

surprising aptness of broad ranges of nucleic acid species to obtain even the idealized states of classical liquid-crystalline mesophases, irrespective of whether polydispersed high-molecular-weight DNAs and RNAs or shorter definite stretches of oligo(deoxy)nucleotides represent the different objects of interest. Contrary to the ease of adopting mesophases, in general, the requirements for evolutionary diversities compared with man-made artificials[2,69–71] render adjustments of definite molecular patterns to rather unspecific, complex texture expressions an open problem. The sequences of Figs 3 and 4 for polydispersed dsDNA, dsRNA, tsRNA and qsRNA mesophase arrangements thus reveal accidental space–time cuts from complex mesophase developments between cholesteric and columnar hexagonal phases,[25,28,48–61,74–76] and spectra of multiple combinations would result from even small differences in starting conditions and sample evolutions. The dsRNA–peptide textures complicate the picture by the multitude of peptide partner interaction facilities that enhance the multiplicity of expressions, even up to possible solution-demixings.[1,2,4–6,34,35,63] It should be emphasized that we are thus unable to follow complex individual mesophase interplays by the common instrumentary of statistical majority descriptions, and that the problems of evolutionary probabilistics themselves exclude full deterministic relationships with well-expressed texture appearances and transition sequences within reproducible phase diagrams. Aside from the elite, highly sophisticated ambitions of countless researchers to elucidate mesophase relationships in close interdependences with molecular and amphotrophic parameters, expressed in pronounced mesophase appearances of definite sequences,[25–32,44–61] the complex basal prerequisites of our systems yielded coloured mosaic patterns of quite different mesophase appearances within complex texture evolutions of each individual system. So it is virtually by chance that if Figs 3 and 4 present texture evolutions they are characterized by probabilistic space–time-dependent mosaics of micropatterns between cholesteric and columnar phases rather than by fully deterministic complete overall designs within well-characterized phase diagrams.[2,74,75]

Scanning force microscopy visualizations of the poly(deoxy)nucleotide (peptide) samples

Although organizational phenomena, especially in artificial liquid crystals, have been compared by SFM and STM, the field of biopolymer species has been devoted mainly to studies of molecular individuals rather than molecular ensembles.[63–113] Here, numerous artificial and native objects—differently stranded nucleic acids, helical superstructures, plasmids, bacteriophages, viruses, proteins and membranes—have been visualized by depositing on a variety of quite different surfaces, such as graphite, (modified) mica, silicon, MoS_2 and various other minerals.[68,69–72,74–76,79,80,83–98] The obvious neglect of mesophase patterns in previous nucleic acid SXM investigations remains surprising in view of the common emphasis and endeavours in biopolymer packings, replications, information processings and general *in vitro* and *in vivo* regulations.[2,73] Our first approaches to SFM elucidation of nucleic acid domain and microdomain self-organizations in adlayers to solid supports unravelled the first intriguing pictures of nano and subnano insights into supramolecular arrangements within self-organizational biomesogen patterns[2,24,74–77] and it had been the elucidations of single-molecule[88] methodologies that turned unexpectedly successful in this case.[74,75] Although graphite, after the first euphoria, had been accused of mimicking the clefts and breaks in nucleic acid design, with its lower adhesion forces to nucleic acids in highly concentrated aqueous solution it provided a rather ideal support to tolerate nucleic acid self-organizations within the slowly evaporating adlayers.[2,74–77] Even the more obtuse pyramidal tips in the convenient contact force mode proved favourable in comparison with the more acute but abrasive versions in the more sensitive tapping mode. Although we used the rolling droplet method on freshly cleaved HOPG, as described previously in detail,[74,75] precaution is to be taken in the interpretation of the images.

All high resolution microscopy studies were performed in the contact mode, with forces of ~20 nN between tip and sample. From SEM images of the Si_3N_4 tips used, we estimate a typical curvature radius R of the tip to be ~25 nm and a full aperture 2α of the tip cone to be 90°. The SFM images of parallel nucleic acid stretches exhibit more structures with details down to ~20 nm, in accordance with the values of R and 2α. This yields a nominal pressure under the tip of ~2 kbar, assuming a depression of the sample caused by the tip of 1 nm. A single strand of nucleic acid is known to have a diameter of ~2.2 nm. From the apparent height of 1.2 nm in the SFM image and the apparent width of the strands, it might be concluded that each visible parallel zig-zag line structure corresponds to either ds/ts/qs-nucleic acids or bundles of such arrangements. In all DNA, RNA and certain RNA/peptide images (Figs 5–7), we notice well-ordered areas of thicker bunches together with neighbouring regions of apparently finer and thinner structures. These finer lines may well correspond to single nucleic acid strands, possibly pulled out of the ordered region of nucleic acid bundles by the action of the SFM tip. Further proof of the image broadening effect by the bluntness of the tip is seen by the substrate steps, which are of monoatomic height but of apparent width 2.3 nm.

The effect of a non-negligible pressure exerted by the tip on the sample has been proved by the observation of an occasional shift of parts of the strand assemblies over a substantial distance in the imaged area, whereas other parts of the strand assembly with seemingly stronger adhesion to the substrate remain unaltered (besides the effect of thermal drift). Owing to their much stronger contrast compared with the height images, predominantly lateral force images are presented here (the weakness of the contrast of the height images results from the larger contrast slope superimposed onto the small nucleic acid structures, caused by the inevitable inclination of the substrate crystal with respect to the axis of the scanning tip). To a rough approximation, a lateral force image might be considered as a derivative of the corresponding

height image taken in the scan direction. In this particular imaging mode, strands of nucleic acid appear lying on the substrate because they would be shaded by glancing incidence light illumination from left or right. Thus, the given figures for the grey level of the lateral force images do not correspond to the real height profile values. Instead, the estimated values for the apparent height (thickness) of the strands are taken from acquired height signal images not shown here.

From this it might be concluded that the observed cholesteric and columnar-like ordering phenomena pre-exist before the first SFM scan takes place and the structure is altered eventually due to occasional fluctuations in the tip–sample interaction. This provides further evidence that the self-organized pattern of nucleic acid strands must be there before the SFM observation starts and is thus very unlikely to be initiated by the SFM scan itself.

Scanning force microscopy of chicken erythrocyte DNA

Figure 5 illustrates a mesophase-derived polydispersed DNA adlayer.[2,74–79,89–98,113] The overall two- and three-dimensional presentations under conditions comparable to near-solid cholesteric and columnar hexagonal mesophase designs[2,27–33,48–66,74–79] are additionally governed by the wall conditions of the originating adlayers and imprinted by the dynamics of the rolling-drop rheology.[2,74,75] On the other hand, single rods, given here in three-dimensions presentation, hint at the building blocks of strand arrangements without being capable of discerning between strands, strand bundles and their possible (intertwinning) packing modes.[1,2,6,7,13,16,34–42] The flexibility of the long dsDNA stretches suitably follows both self-organizational and flow-dictated morphologies (and, curiously and fortuitously, leads back to the possible blueprinting of inorganic matrices for liberated organic matrix generations, reminding us of common principles), the bottom presentation of Fig. 5 also reveals fractality convergences in nucleic acid mesophase with terrestric plate tectonics of a well-known Western Himalaya region.

The resulting images correspond, in the main, to expectations derived from indirect texture mesophase elucidations by polarizing light microscopy. Because near-solid mesophase appearances of nucleic acids (presumed for adlayer conditions) tend to cholesteric and columnar hexagonal mesophases, rather massive packings of the long-shaped molecules will be expected.

Scanning force microscopy of dsRNA- and dsRNA/peptide organizations

Up to quite recently, DNA in SFM and SXM investigations has overshadowed RNA.[2,24,74–82,90–113] The genetic material, its transport through cell membranes, the flexibility and adaptability of the molecules as receptor and effector, antisense strategies, the kingdoms of protein interactions and, last not least, the problems around the human genome project stimulated various permanent SFM/STM enterprises. Favoured in comparison to RNA by its easy accessibility and minor degradability DNA has opened up a lot of routes to all sorts of definite sequences and substitution variations into phosphates, sugars and bases. On the other hand, RNA has suffered from its nuclease sensitivity, the dramatic difficulties of synthesis and the widespread appearances of quite different molecular entities under quite different preconditions.

The SFM imaging in Fig. 6 reveals—for the double- and triple-stranded $(A)_n/(U)_n$ combinations, the quadruple-stranded 'Gs' and, to a certain degree, also the AU duplexes engaged in interactions with short $(L\text{-Lys})_5$ oligopeptides—long stretches of parallel-aligned massive bundles, foreseen, as in the case of DNA by near-solid mesophase appearances of cholesteric and columnar hexagonal arrangements. The RNA is stiffer in comparison to DNA but also, by the lower resolution of our SFM procedure, which is better able to elucidate the organizational relationships than details of the building programmes of the single bundles, the rod-like packages dominate the images.

Different from these visualizations, the triplex images present the molecular constituents as short-plaited grapes with intertwinned strand bundles. As the nucleic acid triplex build-up implies, in our case the subsequent addition of the third Hoogsteen strand to a possibly not perfectly matched preformed duplex,[1,2,6,7,16,18,34–42] the different aberrations of the third partner in inter- and intrastrand interactions and a further step of degradation might well account for the complexity and compactness of the triplex appearances in two- and three-dimensions.

Those 'triplex' imaging relationships reappear to a certain degree in the AU–Lys combinations of the high-molecular-weight Lys partners of 2–15 kDa (Fig. 7). It was just such Lys combinations that, in former days, had attracted attention for the membrane passage of dsRNAs in cytokine induction up to the present interferences of dsRNA signal systems with genome regulations,[1,2,62–64,114] and a multitude of models, including our own in Fig. 1, had been used for detailed suggestions to cope with a complexity of receptor interaction needed by suitable model designs.[1,2,4–6,13,16,22,24,33–42,63] To our knowledge, none of the different proposals has been proved unequivocally and here, with L-Lys-2000 and L-Lys-6000, an increasing tendency for nucleic-acid–triplex-comparable plaited grapes and even toroidal structures appears in the SFM imaging of such dsRNA/high-molecular-weight L-Lys combinations. On the other hand, the high-molecular-weight entities of L-Lys–10000-15000 seem to be dominated by slightly distorted bundles of stretches that might hint at direct interactions of the long-shaped U/A duplexes with the somewhat distorted Lys stretches of the pure L-Lys-2000.[84–87]

Figures 5–7, with their imaging of DNA, RNA- and RNA–Lys domains and microdomains of self-organizational adlayer patterns, set a starting point from which static and even dynamic investigations of self-organizational phenomena of nucleoprotein system components may origin and contribute to a general dual structure–phase view of biomesogen order–disorder patterns between chaotic origin and complexity tensions.

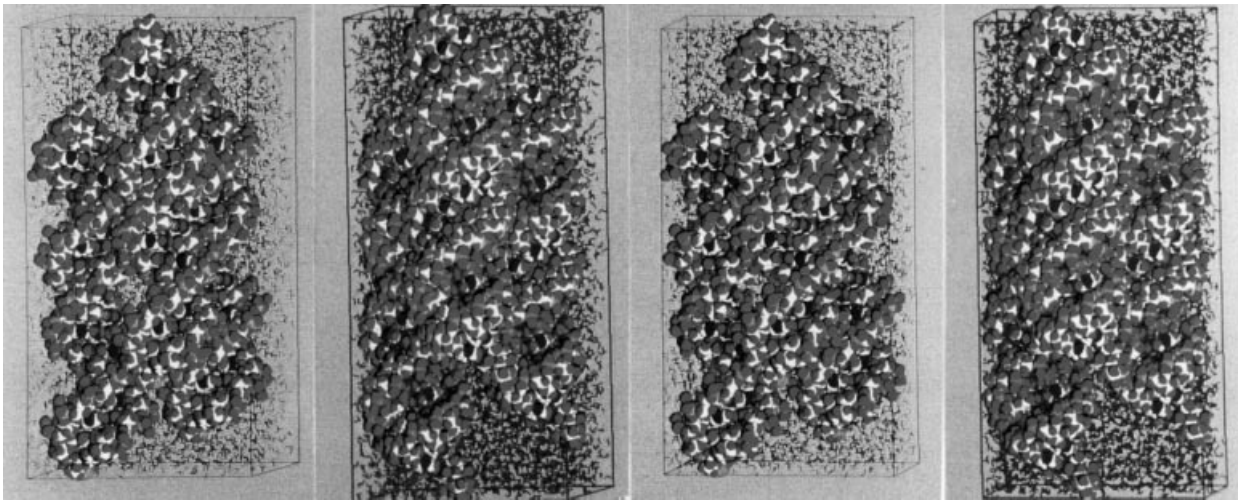

Figure 8. Biomesogen DNA and RNA organizations between 'structure and phase'[1,2] (left to right): B-DNA and A-RNA duplexes in cholesteric and columnar mesophase-derived meso(micro)phase (and adlayer) relevant arrangements.

CONCLUSIONS

In conclusion, scanning probe microscopy, especially SFM and STM, proved highly efficient in the elucidation of single-molecule details. Contrary to recent progress in the imaging of mesophase areas of low-molecular-weight artificials, investigations in the field of biomesogen species and their models are still in their infancy. Scanning force microscopy visualizations of nucleic acid and nucleoprotein adlayer domains and microdomains, preferentially on graphite substrates, offer insight into the operational modes of their self-organizational patterns (Fig. 8). Further progress in statics and dynamics depends on the accessibility of native milieus in liquid cells and hopefully will profit (especially in molecular dynamics) from continuing improvements in the rapidly developing equipment.

The imaging of biomesogen subjects from the perspective of phase cooperativity and complexity contributes to the coherence of the inherent structure/phase dualities.

Acknowledgements

The studies were supported by a grant from the Saxony-Anhalt Ministry of Culture and Education, by the Ministry for Science and Research (Saxony-Anhalt), the Funds of Chemical Industries, the National Employment Office Halle/Saale, EU-INTAS Projects and DAAD Eastpartnerships. The authors gratefully acknowledge the SFM facilities, generously provided by Professors J. Kirschner and U. Gösele at the Max Planck Institute of Microstructure Physics, Halle/Saale.

REFERENCES

1. Hoffmann S. *Molecular Matrices (I Evolution, II Proteins, III Nucleic Acids, IV Membranes)*. Akademie-Verlag: Berlin, 1978.
2. Hoffmann S. In *Handbook of Liquid Crystals/Living Systems*, Demus D, Goodby J, Gray GW, Spiess H-W, Vill V (eds). vol. 3. Wiley-VCH: Weinheim, 1998; 393–452.
3. Hoffmann S, Witkowski W. *Am. Chem. Soc. Symp. Ser.* 1978; **74**: 178.
4. Hoffmann S. In *Polymeric Liquid Crystals*, Blumstein A (ed.). Plenum Press: New York, 1985; 423–452.
5. Samulski ET. *Faraday Discuss. Chem. Soc.* 1985; **79**: 7.
6. Sarma RH. *Nucleic Acid Geometry and Dynamics*. Pergamon Press: New York, 1980; 83–108.
7. Kamath S, Sarma MH, Zhurkin VB, Turner CJ, Sarma RH. *J. Biomol. Struct. Dyn., Convers.* 2000; **11**: 317.
8. Mitra SN, Biswas R, Shi K, Sundaralingam M. *J. Biomol. Struct. Dyn., Convers.* 2000; **11**: 196.
9. Eschenmoser A. *Angew. Chem.* 1988; **100**: 5; *Angew. Chem. Int. Ed.* 1988; **27**: 5; *Orig. Life Evol. Biosph.* 1994; **24**: 389.
10. Ringsdorf H, Schlarb B, Venzmer J. *Angew. Chem.* 1988; **100**: 117; *Angew. Chem. Int. Ed.* 1988; **27**: 113.
11. Lehn J-M. *Supramolecular Chemistry*. VCH: Weinheim, 1995.
12. Lehn J-M. *Science* 1985; **227**: 849.
13. Guschlbauer W. *Encycl. Polym. Sci. Eng.* 1988; **12**: 699.
14. Williams RJP. *Biochem. Soc. Trans.* 1990; 689–705.
15. Schramm G, Grötsch H, Pollmann W. *Angew. Chem.* 1962; **74**: 53; *Angew. Chem. Int. Ed.* 1962; **1**: 1.
16. Olson WK. *Proc. Natl. Acad. Sci. USA* 1977; **74**: 1775.
17. Cech Th. R. *Nature* 1988; **332**: 777.
18. Ackermann. *Angew. Chem.* 1989; **101**: 1005–1016; *Angew. Chem. Int. Ed.* 1989; **28**: 981.
19. Orgel LE. *Nature* 1992; **358**: 203.
20. Hoffmann S. *Angew. Chem.* 1992; **104**: 1032; *Angew. Chem. Int. Ed.* 1992; **31**: 1013.
21. Hoffmann S. In *Organic Synthesis Highlights III*, (Mulzer J, Waldmann H (eds). Wiley-VCH: Weinheim, 1998; 219–226.
22. Hoffmann S. In *Chirality—From Weak Bosons to the α-Helix*, Janoschek R (ed.). Springer-Verlag: Berlin, 1991; 205–238.
23. Siegel JS. *Chirality* 1998; 1024.
24. Hoffmann S. In *Self-Production of Supramolecular Structures*, Fleischaker GR, Colonna S, Luisi PL (eds). *NATO ASI Ser.* 496. Kluwer Academic: Dordrecht, 1994; 3–22.
25. Leforestier A, Fudaley S, Livolant F. *J. Mol. Biol.* 1999; **290**: 481.
26. Strzelecka TE, Davidson MW, Rill RL. *Nature* 1988; **331**: 457.
27. Reich Z, Ittah Y, Weinberger S, Minsky A. *J. Biol. Chem.* 1996; **265**: 5590.
28. Yu., Yevdokimov M, Skuridin SG, Salyanow VI. *Liq. Cryst.* 1988; **3**: 1443.
29. Iizuka E. *Polymer J.* 1978; **10**: 293.
30. Brandes R, Kearns DR. *Biochemistry* 1986; **25**: 5890.
31. Spada GP, Carcuro A, Colonna FP, Garbesi A, Gottarelli G. *Liq. Cryst.* 1988; **3**: 651.
32. Mariani P, Ciuchi T, Saturni L. *Biophys. J.* 1998; **74**: 430.
33. Hoffmann S. *Z. Chem.* 1987; **27**: 395.
34. Guschlbauer W, Chantot J-F, Thiele D. *J. Biomol. Struct. Dyn.* 1990; **3**: 491.

35. Arnott S, Selsing E. *J. Mol. Biol.* 1974; **88**: 509.
36. Felsenfeld G, Rich A. *Biochem. Biophys. Acta* 1957; **26**: 457; *Proc. Natl. Acad Sci. USA* 1977; **74**: 1775.
37. Stevens CL, Felsenfeld G. *Biopolymers* 1964; **2**: 293.
38. Krakauer H, Sturtevant JM. *Biopolymers* 1968; **6**: 491.
39. Michelson AM, Massoulié J, Guschlbauer W. *Prog. Nucleic Acid Res. Mol. Biol.* 1967; **6**: 83.
40. Church ChM, Sussman JL, Kim S-H. *Proc. Natl. Acad. Sci. USA* 1977; **74**: 1458.
41. Carter CW, Kraut J. *Proc. Natl. Acad. Sci. USA* 1974; **71**: 283.
42. Sussman JL, Trifonow EF. *Proc. Natl. Acad. Sci. USA* 1978; **75**: 103.
43. Livolant F. *J. Phys.* 1989; **50**: 1729; *J. Phys.* 1987; **48**: 1051; *J. Phys.* 1987; **47**: 1605.
44. Livolant F. *J. Mol. Biol.* 1991; **218**: 165.
45. Livolant F, Bouligand Y. *Mol. Cryst Liq. Cryst.* 1989; **166**: 91.
46. Leforestier A, Livolant F. *J. Phys. II* 1992; **2**: 1853.
47. Leforestier A, Livolant F. *Biophys. J.* 1993; **65**: 56.
48. Livolant F, Leforestier A. *Progr. Polym. Sci.* 1996; **21**: 1115.
49. Sikorav J-L, Pelta J, Livolant F. *Biophys. J.* 1994; **67**: 1387.
50. Pelta J, Durand D, Doucet J, Livolant F. *Biophys. J.* 1996; **71**: 48.
51. Gulbrand L, Nilsson LG, Nordenskiöld L. *J. Chem. Phys.* 1986; **85**: 6686.
52. Rill RL. *Proc. Natl. Acad. Sci, USA* 1986; **83**: 342.
53. Rill RL, Hilliard PR, Levy GC. *J. Biol. Chem.* 1983; **258**: 250.
54. Rill RL, Strzelecka TE, Davidson MW, van Winkle DH. *Physica A* 1991; **176**: 87.
55. van Winkle DH, Davidson MW, Rill RL. *J. Chem. Phys.* 1992; **97**: 5641.
56. Strzelecka TE Rill. *J. Am Chem. Soc* 1987; **109**: 4513.
57. Strzelecka TE, Rill RL. *Biopolymers* 1990; **30**: 57.
58. Reich Z, Wachtel E, Minsky A. *Science* 1994; **264**: 1460.
59. Reich Z, Levin-Zaidman S, Gutman SB, Arad T, Minsky A. *Biochemistry* 1994; **33**: 14177.
60. Wolf SG, Frenkiel D, Arad T, Finkels SE, Kolter R, Minsky A. *Nature* 1999; **400**: 83.
61. Golo VL, Kats EI, Yu., Yevdokimov M. *J. Biomol. Struct. Dyn* 1998; **15**: 757.
62. Hoffmann S. *Riga Symposium on Bioorganic Chemistry and Drug Design*, Riga, 1982.; *Wiss. Z. Univ. Halle* 1983; **32/4**: 51.
63. Hoffmann S. *Z. Chem.* 1982; **22**: 357; *Z. Chem.* 1979; **19**: 241.
64. Hoffmann S. *Wiss Z. Univ. Halle* 1989; **38**: 3.
65. Meister W-V, Ladhoff A-M, Kargov SI, Burckhardt G, Luck G, Hoffmann S. *Z. Chem.* 1990; **30**: 213.
66. Thondorf I, Lichtenberger O, Hoffmann S. *Z. Chem.* 1990; **30**: 171.
67. Ijiro K, Ringsdorf H, Birch-Hirschfeld E, Hoffmann S, Schilken U, Strube M. *Langmuir* 1998; **14**: 2796.
68. Frommer J. *Angew. Chem.* 1992; **104**: 1325; *Angew. Chem. Int. Ed.* 1992; **30**: 1298.
69. Cincotti S, Rabe JP. *Supramol. Sci.* 1994; **1**: 7.
70. Heinz R, Rabe JP, Meister W-V, Hoffmann S. *Thin Solid Films* 1995; **264**: 246.
71. Eichhorst-Gerner K, Stabel A, Moessner G, Declerq D, Valiyaveettil S, Enkelmann V, Müllen K, Rabe JP. *Angew. Chem.* 1996; **108**: 1599; *Angew. Chem. Int. Ed.* 1996; **35**: 1492.
72. Seeman NC. *Angew. Chem* 1998; **110**: 3408; *Angew.Chem Int. Ed.* 1998; **37**: 3220.
73. Lehn J-M. *Eur. J. Chem.* 1999; **5**: 2443.
74. Bohley C, Matern D, Bischoff G, Meister W-V, Kargov S, Lindau S, Barthel J, Hoffmann S. *Surf. Interface Anal.* 1997; **25**: 614.
75. Bohley C, Martini T, Bischoff G, Lindau S, Birch-Hirschfeld E, Kargov S, Meister W-V, Barthel J, Hoffmann S. *Nucleos. Nucleot.* 1997; **16**: 2013.
76. Bohley C, Meister W-V, Bischoff G, Bischoff R, de S, Bambirra A, Lindau S, Kargov S, Barthel J, Hoffmann S. *J. Biomol. Struct. Dyn.* 1997; **14**: 827.
77. Meister W-V, Kargov SI, Birch-Hirschfeld E, Bohley C, Burckhardt G, Bischoff G, Bischoff R, Gromann U, Hoffmann S. *Nucleos. Nucleot.* 1998; **17**: 1905.
78. Kovalenko L, Lindau S, Bohley C, Panchenko N, Meister W-V, Zhuk R, Hoffmann S. *Nucleos. Nucleot.* 1998; **17**: 1813.
79. Bischoff G, Bischoff R, Birch-Hirschfeld E, Gromann U, Lindau S, Meister W-V, de S, Bambirra A, Bohley C, Hoffmann S. *J. Biomol. Struct. Dyn.* 1998; **15**: 187; *J. Biomol. Struct. Dyn.* 1997; **14**: 175.
80. Meister W-V, Lindau S, Hauser AL, Bohley C, Gromann U, Madre M, Kovalenko L, Bischoff G, Zhuk R, Hoffmann S. *J. Biomol. Struct. Dyn.* 1999; **16**: 1312; *J. Biomol. Struct. Dyn.* 2000; **18**: 385.
81. Bischoff G, Gromann U, Lindau S, Meister W-V, Hoffmann S. *Nucleos. Nucleot.* 1999; **18**: 2201.
82. Bischoff G, Gromann U, Lindau S, Bischoff R, Bohley C, Meister W-V, Hoffmann S. *J. Biomol. Struct. Dyn.* 1999; **16**: 1308; *J. Biomol. Struct. Dyn.* 2000; **18**: 199.
83. Haynes M, Garrett RA, Gratzer WB. *Biochemistry* 1970; **9**: 4410.
84. Tsubai M, Matsuo K, Ts'o POP. *J. Mol. Biol.* 1966; **15**: 256.
85. Azorin A, Vives J, Campos JL, Jordan A, Lloveras J, Puigjanev L, Subirana JA, Mayer R, Brack A,*J. Mol. Biol.* 1985; **185**: 371.
86. Hud NV, Downing KH, Balhorn R. *Proc. Natl. Acad. Sci, USA* 1995; **92**: 3581.
87. Allen MJ, Tench RJ, Mazrimas JA, Balooch M, Siekhaus WJ, Balhorn R. *Scanning Microsc.* 1993; **7**: 563.
88. Clemmer CR, Th, Beebe P. *Science* 1991; **251**: 640.
89. Zasadzinski JAN, Schneir J, Gurley J, Elings V, Hansma PK. *Science* 1988; **239**: 1013.
90. Bezanilla M, Manne S, Laney DE, Lyubchenko YL, Hansma HG. *Langmuir* 1995; **11**: 655.
91. Hansma HG, Revenko I, Kim K, Laney DE. *Nucleic Acids Res.* 1996; **24**: 713.
92. Hansma HG, Pietrasanta LI, Golan R, Sitko JC, Viani MB, Paloczi GT, Smith BL, Throver D, Hasma PK. *J. Biomol. Struct. Dyn., Convers.* 2000; **11**: 271.
93. Janshoff A, Neitzert M, Oberdörfer Y, Fuchs H. *Angew. Chem.* 2000; **112**: 3346; *Angew. Chem. Int. Ed.* 2000; **39**: 3212.
94. Coratger R, Chahboun A, Ajustron F, Beauvillain J, Erard M, Amalric F. *Ultramicroscopy* 1990; **34**: 141.
95. Thundat T, Allison DP, Warmack RJ, Ferrell TL. *Ultramicroscopy* 1992; **42–44**: 1101.
96. Thundat T, Zheng X-Y, Sharp SL, Allison DP, Warmack RJ, Joy DC, Ferrell TL. *Scanning Microsc.* 1992; **6**: 903.
97. Thundat T, Allison DP, Warmack RJ, Doktycz MJ, Jacobson KB, Brown GM. *J. Vac. Sci. Technol. A.* 1993; **11**: 824.
98. Thundat T, Warmack RJ, Allison DP, Jacobson KB. *Scanning Microsc.* 1994; **8**: 23.
99. Ziady A-G, Ferkol Th, Dawson DV, Perlmutter DH, Davis DB. *J. Biol. Chem.* 1999; **274**: 4908.
100. Dunlap DA, Maggi A, Soria MR, Monaco L. *Nucleic Acid Res.* 1997; **25**: 3095.
101. Lin Z, Wang C, Feng X, Liu M, Li J, Bai C. *Nucleic Acids Res.* 1998; **26**: 3228.
102. Ohlenbusch HH, Bosshard HE. *Nanotechnology* 1993; **4**: 91.
103. Hummer G, Garcia AE, Soumpases DM. *Biophys. J.* 1995; **68**: 1639.
104. Lyubchenko YL, Shlyakhtenko LS, *Proc. Natl. Acad. Sci. USA* 1997; **94**: 496.
105. Lyubchenko YL, Oden PI, Lampner D, Lindsay SM, Dunker KA. *Nucleic Acids Res.* 1993; **21**: 1117.
106. Lindsay SM, Lyubchenko YL, Tao NJ, Li YQ, Oden PI, DeRose JA, Pan J. *J. Vac. Sci. Technol. A* 1993; **11**: 808.
107. Shaiu W-L, Larson DD, Vesenka J, Henderson E. *Nucleic Acids Res.* 1993; **21**: 99.
108. Feigon J, Smith FW, Mayer RF, Schultze P. In *Structural Biology II*, Sarma RH, Sarma MH (eds). Adenine Press: Schenectady, NY, 1994; 127–134.
109. Delain E, LeCam E, Barbin A, Bargain-Arbogast A, Fourcade R. *Microsc. Microanal. Microstruct.* 1994; **5**: 329.
110. Draper DE. *J. Mol. Biol.* 1999; **290**: 255.

111. Hölscher H, Schwarz UD, Zwörner O, Wiesendanger R. *Phys. Rev. B* 1998; **57**: 2477.
112. Marsh ThC Vesenka E, Henderson J. *Nucleic Acids Res.* 1995; **23**: 696.
113. Takano H, Kenseth JR, Wong S-S, O'Brien JC, Porter MD. *Chem. Rev.* 1999; **99**: 2845.
114. Schepers U, Kolter T. *Angew. Chem.* 2001; **113**: 2503; *Angew. Chem. Int. Ed.* 2001; **40**: 2437.